Available online at www.sciencedirect.com
SCIENCE DIRECT®
International Journal of Heat and Fluid Flow 26 (2005) 746–754
International Journal of HEAT AND FLUID FLOW
www.elsevier.com/locate/ijhff

Multiple flow patterns and heat transfer in confined jet impingement

Xianchang Li [a,*], J. Leo Gaddis [b,1], Ting Wang [a,2]

[a] Energy Conversion and Conservation Center, University of New Orleans, New Orleans, LA 70148-2220, USA
[b] Department of Mechanical Engineering, Clemson University, Clemson, SC 29634-0921, USA

Received 21 February 2004; accepted 26 January 2005
Available online 25 March 2005

Abstract

The flow field of a 2-D laminar confined impinging slot jet is investigated. Numerical results indicate that there exist two different solutions in some range of geometric and flow parameters. The two steady flow patterns are obtained under identical boundary conditions but only with different initial flow fields. Two different exit boundary conditions are investigated with two commercial software packages to eliminate artificial or computational effects. The different flow patterns are observed to significantly affect the heat transfer. A flow visualization experiment is carried out to verify the computational results and both flow patterns are observed. The bifurcation mechanism is interpreted and discussed.

Keywords: Flow patterns; Confined jet; Impingement; Heat transfer

1. Introduction

Because of its high heat and mass transfer rate, jet impingement has been used in many industrial fields, for example, annealing of metal and plastic sheets, cooling of gas turbine blades and electronic components, etc. Numerous studies have been conducted on jet impingement flow and heat transfer. Most of the studies reported parametric influence on the local heat transfer coefficient or methods to enhance the heat transfer. Detailed topics included the effects of the jet Reynolds number, nozzle configuration, turbulent intensity, and target spacing. For example, Sparrow and Wong (1975) measured mass transfer coefficients of a slot jet impinging on a plane surface, and then converted to heat transfer coefficients. The shape of the initial velocity profile was found significant on the heat transfer characteristics of the impinging surface. Extensive reviews on jet impingement study prior to 1992 have been given by Martin (1977) and Jambunathan et al. (1992), and will not be repeated here. Recognizing that it is the flow field that governs the heat transfer between the jet fluid and the target wall, the study of the flow field is essential. van Heiningen et al. (1976) predicted numerically the flow fields of a laminar impinging slot jet. Their emphasis was on the effects of uniform suction to the target wall and nozzle exit velocity profile on the flow and heat transfer characteristics. Chou and Hung (1994) numerically studied the flow field of a 2-D confined impinging slot jet. They presented the effects of the jet Reynolds number, the velocity profile at the jet exit, and the distance between jet and target wall on heat transfer. Garimella and Rice (1995) presented some sketches of visualized streamlines for the flow fields of a confined impinging round jet. A toroidal recirculation pattern was identified, which became larger when the target distance was increased. The emphasis of their work was also on the effects of the nozzle-to-target spacing, Reynolds number and nozzle diameter on heat transfer. Morris et al. (1996) studied numerically the

* Corresponding author. Tel.: +1 504 280 6032.
E-mail addresses: xli8@uno.edu (X. Li), leo.gaddis@ces.clemson.edu (J.L. Gaddis), twang@uno.edu (T. Wang).
[1] Tel.: +1 864 656 3294.
[2] Tel.: +1 504 280 7183.

0142-727X/$ - see front matter © 2005 Elsevier Inc. All rights reserved.
doi:10.1016/j.ijheatfluidflow.2005.01.005

Nomenclature

b	width of slot, m	Pr	Prandtl number
C_p	pressure coefficient $= (p - p_{in})/0.5\rho V_{in}^2$	T	temperature, K
c_p	specific heat, kJ/kg K	T_0	ambient temperature, K
H	spacing between nozzle and target wall, m	T_w	wall temperature, K
h	heat transfer coefficient, W/m^2 K	Re	Reynolds number $= V_{in}b/v$
H'	height of the extended part, m	u, v	velocity components, m/s
k	heat conductivity, W/m K	V_{in}	inlet velocity, m/s
L	length of the flow channel, m	x, y, z	co-ordinates, m
L'	length of the extended part, m	μ	dynamic viscosity, kg/m s
Nu	Nusselt number $= hb/k$	v	kinematic viscosity, m^2/s
p	pressure, N/m^2	ρ	density, kg/m^3
p_{in}	jet inlet pressure, N/m^2		

flow field of an axisymmetric confined jet using a modified k–ε model. The toroidal recirculation patterns in the confinement region of the impinging jet were predicted. They also studied the flow patterns inside the nozzle and the small chamber just before the nozzle. However, their model failed to predict the secondary counter-rotating recirculation patterns observed in their visualization experiments. Chiriac and Ortega (2002) simulated the flow and heat transfer in a transitional confined slot jet impinging on an isothermal surface. The flow was found to become unsteady at a Reynolds number around 600. In the steady regime, the distribution of heat transfer in the wall region was influenced by flow separation caused by the re-entrainment of the spent flow back into the jet. The time-averaged heat transfer in the unsteady regime was stronger than that in the absence of jet unsteady effects. Chung and Luo (2002) studied the heat transfer of a confined impinging jet using direct numerical simulation (DNS). The instantaneous flow fields and heat transfer distributions were found to be highly unsteady and oscillatory in nature, especially for high Reynolds numbers. Laminar jet impingement has also been simulated by Sezai et al. (2004) with a focus on 3-D square jet or jet array.

As part of the work for designing an experimental rig for the mist/steam jet cooling research (Li et al., 2001), we investigated the flow field and heat transfer in a confined slot jet. Numerical results indicate that there are two possible flow patterns depending on the Reynolds number and channel geometry: In some cases, the main flow exits the channel along the target wall and the entrainment flow comes in along the jet plate as a reverse flow; in other cases, the main flow separates from the target wall and a reverse flow occurs along the target wall near the exit. It is interesting to discover that in some range of geometric and flow parameters these two flow patterns coexist at the same boundary conditions. In another word, there exist non-unique solutions for a given problem. The detection of two flow patterns under the same boundary conditions for jet impingement is important for engineering application because the different flow patterns will significantly affect the heat transfer. Particularly, the flow in the downstream half of the channel needs to be carefully considered when the flow might separate from the surface. A flow visualization experiment is carried out in this study to verify the computational results and both flow patterns are observed.

This paper is to investigate the conditions under which the flow patterns coexist and to examine the effect of the flow patterns on heat transfer.

2. Numerical modeling and procedure

2.1. Numerical model

The geometric boundaries and physical conditions are assumed to be symmetric about the centerline of the jet; therefore, only half the physical domain is considered in numerical models. The impinging jet system is shown in Fig. 1. Two domains have been used to facilitate examining the effect of exit boundary condition since it is of concern that the solution may be sensitive to the assumed boundary conditions at the channel exit. The width of the jet nozzle is b. The ratio of the height of the channel to the width of the jet, H/b, is equal to 2.5 and the ratio of the length of the channel over the width of the nozzle, L/b, is equal to 10. To study the effect of geometry on flow fields, larger H/b up to 5 is also considered. Selection of these parameters is based on the analysis that under these conditions the confined wall may strongly affect the jet flow. The dimensions for the extended domain in Fig. 1b are: $H'/b = 15$ and $L'/b = 10$, with which the flow exit is considered far away enough from the position with $x/b = 10$.

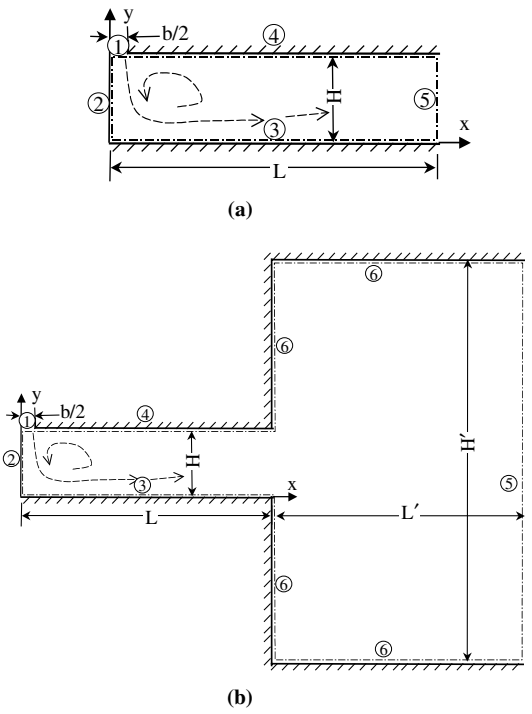

Fig. 1. Computational domain and boundaries. (a) Domain 1, (b) domain 2.

The following assumptions and boundary conditions have been specified: Boundary 1 is the jet inlet ($0 < x < b/2$ and $y = H$). Jet flow is at a uniform velocity ($u = 0$ and $v = V_{in} < 0$) and constant temperature ($T = T_0$). Boundary 2 is the symmetric line ($x = 0$) where $u = 0$, $\partial v/\partial x = 0$, and $\partial T/\partial x = 0$, assuming the velocity and temperature have a smooth distribution along the x-direction. Boundary 3 is the target wall ($y = 0$) and no-slip condition ($u = v = 0$) is applied. The wall is assigned at constant temperature ($T = T_w$). Boundaries 4 and 6 are the confined walls, where no-slip and adiabatic conditions are applied.

At the channel exit (Boundary 5, $x = L$ in Fig. 1a and $x = L + L'$ in Fig. 1b), a constant pressure is applied: p = constant. The thermal boundary conditions at the channel exit are: $T = T_0$ if $u < 0$, or $\partial T/\partial x = 0$ if $u >= 0$, which means that if there is a reverse flow to the channel, the reverse flow will be at the constant ambient temperature; otherwise the temperature gradient will be zero.

2.2. Numerical procedure

Two computational codes have been used in the study to solve the continuity, momentum and energy equations for a laminar flow.

$$\frac{\partial u}{\partial x}+\frac{\partial v}{\partial y}=0 \tag{1}$$

$$\rho\left(u\frac{\partial u}{\partial x}+v\frac{\partial u}{\partial y}\right)=-\frac{\partial p}{\partial x}+\mu\left(\frac{\partial^2 u}{\partial x^2}+\frac{\partial^2 v}{\partial y^2}\right) \tag{2}$$

$$\rho\left(u\frac{\partial v}{\partial x}+v\frac{\partial v}{\partial y}\right)=-\frac{\partial p}{\partial y}+\mu\left(\frac{\partial^2 u}{\partial x^2}+\frac{\partial^2 v}{\partial y^2}\right) \tag{3}$$

$$\rho c_p\left(u\frac{\partial T}{\partial x}+v\frac{\partial T}{\partial y}\right)=k\left(\frac{\partial^2 T}{\partial x^2}+\frac{\partial^2 T}{\partial y^2}\right) \tag{4}$$

The commercial software package Fluent (version 6.1.22) from Fluent, Inc. is used in this study. The simulation uses the segregated solver, which employs an implicit pressure-correction scheme. The SIMPLE algorithm (Patankar, 1980) is used to couple the pressure and velocity. Second order upwind scheme is used for spatial discretization of the convective terms. Another commercial code, PHOENICS, is also used in this study. The reason for using two different codes is to crosscheck the results because the calculation is involved with flow instability, which is sensitive to computational methodologies and associated disturbances. Since both the commercial codes have been well established for a single-phase flow and simple geometry as studied in this paper, descriptions and qualifications of these two codes are not detailed here.

Convergence of the iterative solution has been insured when the residual of all the variables is less than the specified values. The specified value is 10^{-4} for continuity and momentum, and 10^{-6} for energy. The solutions obtained by FLUENT were tested for grid independence by solving the problem with 50, 100, and 200 horizontal meshes (x-direction). As seen in Fig. 2, a structured but nonuniform mesh is used in this study with more grids allocated close to the impinged wall and jet inlet. The number of the vertical meshes (y-direction) is the half of the horizontal meshes. It was found that with 100 horizontal meshes the calculations were essentially grid independent. Fig. 3 shows the pressure coefficient, C_p, along the impinged wall surface of the first computational domain and $Re = 275$, under different grid systems, where C_p is defined as $(p - p_{in})/0.5\rho V_{in}^2$. No perceptible difference exists between the last two grid systems, especially in the region near the stagnation point. A similar procedure was also used to check the grid independence with PHOENICS and the similar conclusion was obtained. As a reference, a grid of 32×46 was used in Chou and Hung (1994), and a grid

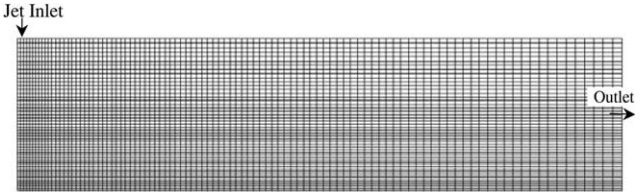

Fig. 2. Structured nonuniform mesh.

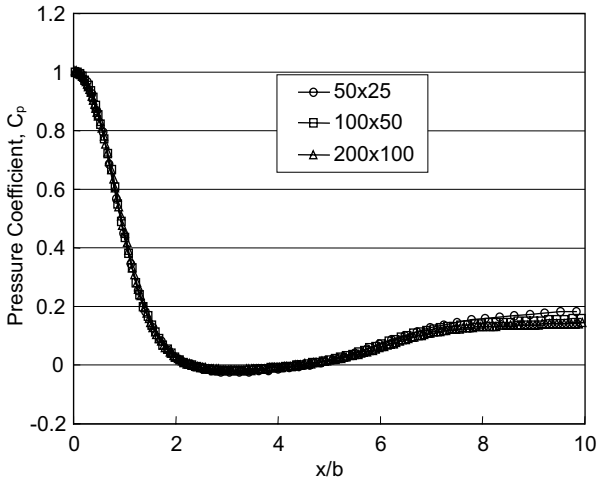

Fig. 3. Effect of grid number on pressure coefficient ($Re = 275$).

of 256×128 was used in Chung and Luo (2002) for direct numerical simulation (DNS). In this study a grid of 100×50 was used.

3. Numerical results and discussions

3.1. Study of a typical case with two flow patterns

A typical flow field given by Fluent for Domain 1 (Fig. 1a) with $L/b = 10$ and $Re = 275$ is shown in Fig. 4a. A large vortex is seen in the confined channel with a separation point occurring on the target wall at about $x/b = 5.5$. The flow separation is mainly due to the suction (or entraining) effect of the jet near the jet exit. The flow at the outlet of the channel contains a reverse flow. The dashed lines with arrowheads were added in Fig. 4a to aid in clarifying the main flow direction. To prove the pattern is indeed a solution, the mass balance is checked to be within a 10^{-5}% between the inlet and outlet mass

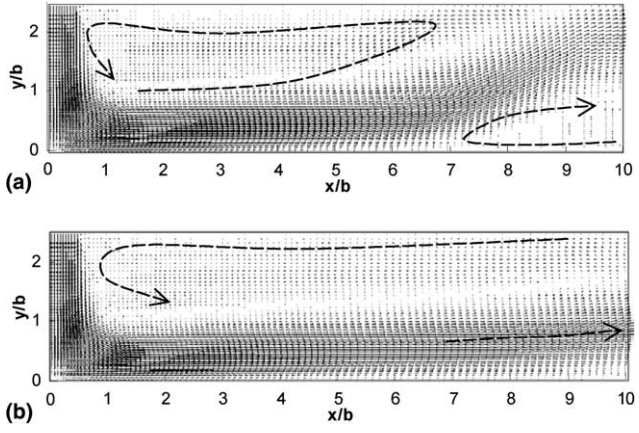

Fig. 4. Flow fields at $Re = 275$ for domain 1 with Fluent. (a) Curved flow pattern, (b) straight flow pattern.

flow rates. Energy conservation has also been checked: the balance of energy entering and leaving the whole domain is 99.89%. A similar flow pattern with the presence of vortex was obtained by Morris et al. (1996) for a 2-D axisymmetric turbulent jet flow. This flow pattern seems reasonable for a pressure-driven flow.

Using a different initial flow field to start iteration, another solution under the same boundary conditions as above has been obtained and is indicated in Fig. 4b. The two solutions are different in significant ways: for the first one, the flow separates from the target wall with a curved pattern; the flow for the second one simply exits as a type of wall jet (straight pattern). However, these two solutions are nearly identical in the stagnation region. The second prediction is also evaluated intensively and it demonstrates the properties of a genuine solution: scrutiny of various internal details such as conservations of mass, momentum, and energy shows that they are all within 1% of reference quantities. It is consequently concluded that two computed solutions are possible.

In this study, two flow patterns were usually obtained by different initial approximations of the flow field. Under the current geometric conditions ($H/b = 2.5$ and $L/b = 10$) and starting with an initial flow field with zero velocity, the results show a curved flow pattern for most of the Reynolds numbers studied. With larger jet-to-target spacing, $H/b > 5$, a zero initial flow field leads to a straight flow pattern. Using the converged result of a straight flow pattern as the initial condition, a straight flow pattern is obtained for a smaller jet-to-target spacing by scaling down the jet-to-target spacing progressively from $H/b > 5$, and repeating this process until $H/b = 2.5$ gives the solution of the straight pattern shown in Fig. 4b. Different approaches can be used to obtain these two solutions, which may depend on the software or the initial flow field used. For example, with a fixed domain size, the solution of one Reynolds number can be manipulated by multiplying a factor to all the velocity components, and then used as the initial condition for the case of another Reynolds number.

To further study the difference between these two solutions, a computation of viscous dissipation rate, which is defined as the summation of $\mu[(\partial u/\partial y)^2 + (\partial v/\partial x)^2]$ at every control volume divided by the inlet kinetic energy, is performed. The results indicate that the straight flow pattern produces a slightly higher value of dissipation than the curved flow pattern, which might mean that the curved flow pattern is a more stable solution. In the real situation, the coexisting condition of these two flow patterns is more delicate. One flow pattern may switch to another one by a subtle disturbance, or the two flow patterns may stay at a steady state for a short time and keep switching from one to another. However, as found by Chiriac and Ortega (2002), the unsteady flow for a confined jet happens when the Reynolds number reaches about 600.

Theoretically, non-unique solutions can also be found in many other problems due to the non-linearity of the Navier–Stokes equations. For example, there are two solutions (symmetric and non-symmetric) for the flow fields in a two-dimensional channel with discontinuous expansions. Battaglia et al. (1997) studied this problem numerically, focusing on how the channel expansion ratio influences the solutions. Their results showed that the critical Reynolds number at which the bifurcation appears decreases with increasing the expansion ratio. Borgas and Pedley (1990) studied high-Reynolds-number steady flow in an annular pipe that encounters a shallow axisymmetric expansion or indentation in the wall using interactive boundary-layer theory. They found that three different solutions could be obtained in an expansion with an adverse pressure gradient larger than a critical value. Jiang and Shen (1994) numerically investigated the bifurcation of confined swirling flow. They found that both low-swirl and high-swirl flow patterns might exhibit at certain swirl levels by gradually changing the swirl level from high to low or from low to high. The bifurcation problem has been also addressed in many other studies (Jayanti and Hewitt, 1992; Orfi et al., 1999) although most of study did not discuss the effect of flow pattern on heat transfer.

3.2. Effects of Reynolds number and geometric parameters

The extent of the parameter range having non-unique solution is investigated by using Fluent software package. With Domain 1 and $H/b = 2.5$, the lowest and highest Reynolds numbers at which two solutions coexist are 275 and 400, respectively. The curved flow pattern persists at lower Reynolds numbers and there is no reverse flow at the channel exit when Reynolds number is small enough (<200), as shown in Fig. 5. At very low Reynolds number of 20, only part of the jet near the stagnation region reaches the target wall. The rest of the jet quickly diffuses and occupies the entire channel, similar to a channel flow.

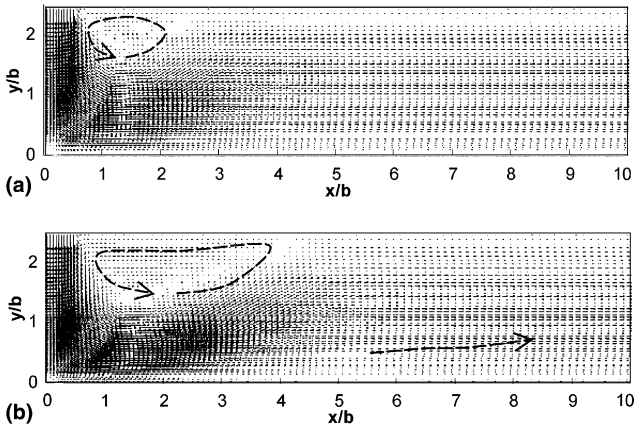

Fig. 5. Flow patterns at low Reynolds number. (a) $Re = 20$, (b) $Re = 100$.

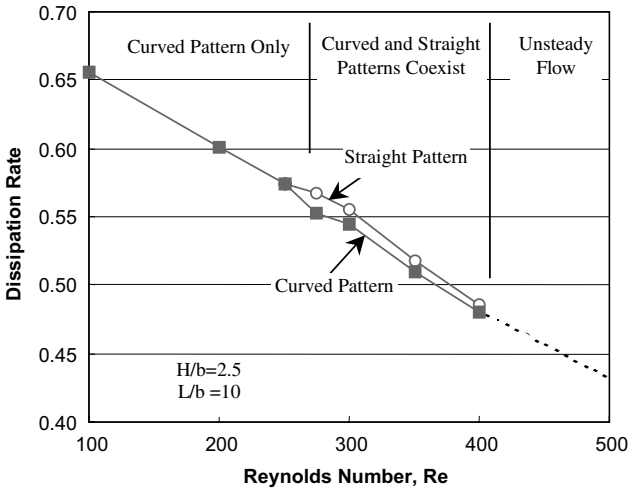

Fig. 6. Dissipation rates under different flow patterns.

As the Reynolds number increases, the extent of the curved flow pattern increases slightly and the boundary layer over the target wall for the straight flow pattern becomes thinner, but the overall patterns are largely unchanged. Fig. 6 shows the overall dissipation rate for all the cases. As mentioned earlier, the dissipation from the straight flow pattern is slightly higher than that from the curved flow pattern. When the Reynolds number reaches above 400, iterations become oscillating and it is believed that the jet impingement flow becomes unsteady, as documented in other studies (Chiriac and Ortega, 2002).

The range of the jet-to-target spacing where both solutions exist is also investigated. For Domain 1 and $Re = 300$, the highest value of H/b is 4.7, and the lowest value is 2.5. H/b values larger than this range always display the straight flow characteristics, and H/b values smaller than this range always display the curved flow characteristics. For each different Reynolds number, there exists a different range for the jet-to-target distance where two solutions coexist. For example, the lowest H/b is 2.6 and 3 for Reynolds number of 250 and 200, respectively. Certainly, the channel length is also an independent parameter worth of study, although this paper only studies a fixed value of $L/b = 10$. A summary of all the cases is given in Table 1.

3.3. Further validation with different software and computational domain

To eliminate any artificial or computational effects due to numerical methodologies or the boundary condition at the channel exit, a second commercial software, PHOENICS, is used to run the cases in both Domains 1 and 2. Using the enlarged domain, the flow at the

Table 1
Summary of the overall results

Cases		Curved pattern	Straight pattern	Note
Effect of Reynolds number (L/b = 10, H/b = 2.5)	20–100	Yes	No	No reverse flow at the channel exit
	200, 250	Yes	No	Reverse flow at the channel exit
	275–400	Yes	Yes	Two patterns coexist
	>400	No	No	Unsteady flow
Effect of target distance H/b (L/b = 10, Re = 300)	<2.5	Yes	No	
	2.5–4.7	Yes	Yes	Two patterns coexist
	>4.7	No	Yes	

channel exit (x/b = 10) is computed rather than specified as the constant-pressure boundary condition. Therefore, the flow field inside the channel will be less affected by the boundary condition given at x/b = 20. As expected, the duplicity of the solution is also predicted by PHOENICS. Figs. 7 and 8 demonstrate both the curved and straight flow patterns calculated by PHOENICS in these cases.

Note that in these two figures the Reynolds numbers are 300 and 350, respectively. It is also worthy noting that the characteristics of main flow swaying to the bottom wall are also shown in cases of enlarged domain in Fig. 8. Since the results using different software and computational domains are identical, it can be suggested that the duplicity of the solution is robust.

3.4. Effect of flow patterns on heat transfer

One important objective of the study of flow patterns is to examine the effect on heat transfer. Fig. 9 shows the heat transfer coefficient distributions for the two typical flow patterns. Beginning at the stagnation point, the heat transfer coefficient decreases rapidly along the target wall for both flow patterns. This similarity of heat transfer between two flow patterns is due to the similar

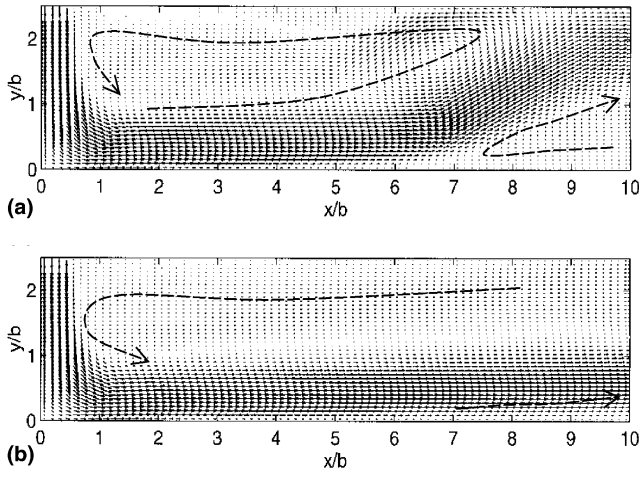

Fig. 7. Flow fields at Re = 300 for domain 1 with PHOENICS. (a) Curved flow pattern, (b) straight flow pattern.

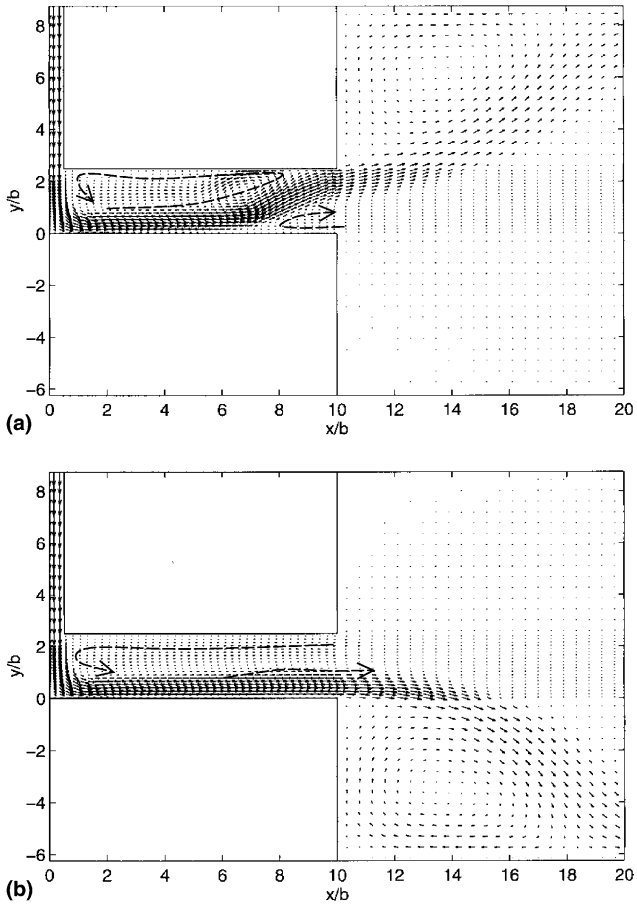

Fig. 8. Flow fields at Re = 350 for domain 2 with PHOENICS. (a) Curved flow pattern, (b) straight flow pattern.

fluid dynamic behaviors in this region. The main difference in the heat transfer behavior between these two flow patterns is found in the downstream half of the channel; whereas the heat transfer coefficient decays steadily for the straight flow. The curved flow pattern produces a lower heat transfer coefficient than the straight flow downstream of the separation point (x/b = 5.5). From the stagnation point to the exit (x/b from 5.5 to 10), the target wall is exposed to a reverse flow entering the normal exit. The reverse flow is assigned the same temperature as the jet, though its value is application dependent. Because the reverse flow has a new

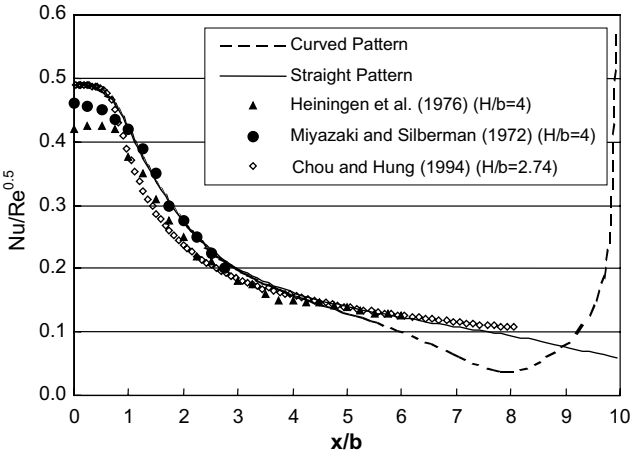

Fig. 9. Heat transfer coefficient for different flow patterns (domain 1 at $Re = 275$).

thermal starting length at $x/b = 10$ (new boundary layer), it produces a high heat transfer coefficient near the exit as shown.

However, the heat transfer of the curved flow pattern in the region $6 < x/b < 9$ is potentially much lower than that indicated without the reverse flow. For example, the heat transfer coefficient at $x/b = 8$ is lower by a factor of approximately 3 than the straight-flow cases. This large heat transfer difference is a prime concern in applications containing the possibility of multiple solutions.

Fig. 9 also shows the results from other research groups (van Heiningen et al., 1976; Miyazaki and Silberman, 1972; Chou and Hung, 1994). The result of this study agrees with others' results well. Notice that the results of other studies follow the trend of the straight flow pattern rather than the curved flow pattern. The values of H/b are different in these studies, which can affect the heat transfer results. Further study shows that the relationship of the Nusselt number at the stagnation point fits the correlation $Nu/Re^{0.5} = \text{constant}$, which agrees with the theoretical analysis of the stagnation flow.

4. Experimental setup and flow visualization

The predictions described are so piquant that we are compelled to seek experimental evidence. An experiment is set up to test for the physical existence of the two solutions. As shown in Fig. 10, this system is mainly for implementing flow visualization; no detailed measurements are intended but the flow rate. The test section is designed according to the dimensions used in the numerical study ($b = 4$ mm, $H/b = 2.5$, and $L/b = 10$). The channel width (in the z-direction, not shown in the figure) is 80 mm and its sidewalls are constructed of clear Plexiglas. The small chamber upstream of the slot is to make the jet flow more uniform. Compressed

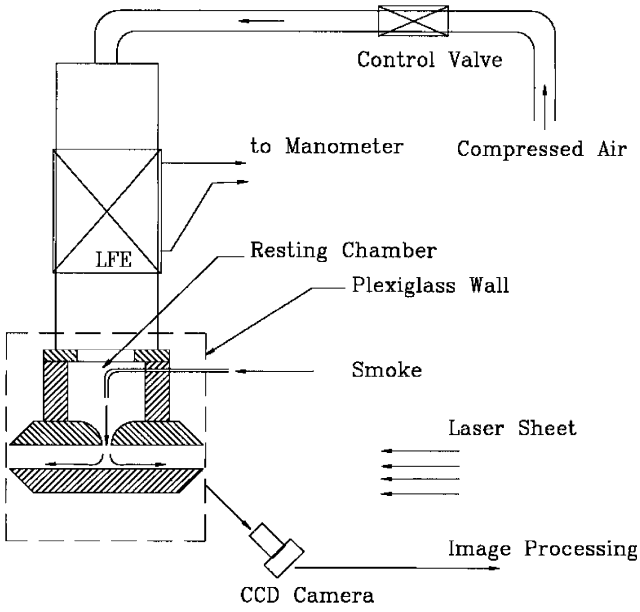

Fig. 10. Experiment setup for flow visualization.

air is admitted through a control valve and measured by an LFE (laminar flow element) and a manometer. The airflow from the test section was exhausted to the ambient. Smoke is injected to the main flow in the small chamber through a small tube with a diameter of about 1mm. The flow field is illuminated by a laser sheet along the central plane in the z-direction and the flow pattern is recorded by a CCD camera.

The two flow patterns are observed in the subject experiment. Streakline pattern records are shown in Fig. 11a and b to attest that these patterns both occur. The Reynolds number is approximately 240 at the condition shown. These patterns are essentially as indicated by the computational predictions, though the smoke only illuminates portions of the primary trace. Prior to testing there was concern on how the switch from one to another pattern could be triggered. It is found that the switch between two flow patterns occurs quite spontaneously when both solutions are possible. No portion of the experiment is adjusted to achieve the records in Fig. 11a and b for a long time. The patterns are established readily and appear to be bistable. The pattern could remain stationary with a period ranging from half a second to more than 10 s before it switches to the second pattern.

At slightly higher Reynolds number values, on some occasions, the flow demonstrates an oscillation of order 10 Hz in which the primary jet deviates transversely. Then at some higher Reynolds number, approximately 400, the flow would display definite three-dimensional turbulent bursts and the flow within the test apparatus would clearly be unstable. More accurate control and equipment are needed to maintain the essential laminar condition.

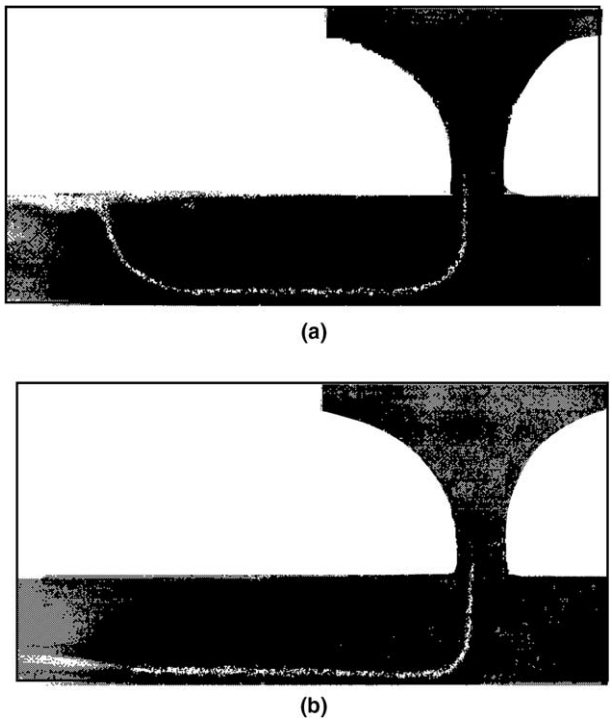

Fig. 11. Streakline pattern from visualization experiment.

In the first runs of the apparatus, the device seems to show a preference for the curved flow solution. Several observational hours are invested before the straight pattern is clearly evident during which time several methods are explored to encourage it. At one variation the target wall is relocated very slightly (1 mm) further from the nozzle wall. The straight flow pattern emerges strongly and the curved flow pattern vanishes despite efforts to encourage it by blocking the exit. In a subsequent run sequence, a piece of polyester filter is placed in the chamber with the target wall restored to its normal position. Only the straight flow pattern could be produced. Upon removal of the filter, both patterns are spontaneous. It is inferred from these observations that the patterns are only marginally stable though they can occur for indefinite periods and are not particularly subject to change by blocking of selective sides of the exit channel.

5. Conclusions

The flow fields of a 2-D laminar confined impinging jet have been numerically investigated. The effects of the jet Reynolds number, the geometric relationships of the jet impingement system and the boundary conditions on the flow patterns have been examined. The major conclusions from the present study are as follows:

1. The confined impinging jet flow shows two different flow patterns: a curved flow pattern and a straight flow pattern. In some cases, the two patterns coexist under the same conditions. Two numerical solutions can be obtained with different initial flow approximations.
2. The flow patterns mainly depend on the Reynolds number and geometry. The boundary conditions of numerical solutions at the channel exit exert minor changes on the flow.
3. The dynamic and thermal behaviors are similar in the stagnation region for both flow patterns. The flow patterns affect significantly the heat transfer for the downstream half of the target surface. Variations of a factor of three are predicted for the local heat transfer coefficient at a highly sensitive position. It is important to be aware of the consequence of this variation in heat transfer coefficient when a similar arrangement is used to cool a heated surface.
4. Two flow patterns have been verified by flow visualization indicating agreement with numerical predictions. The experimental range of flow rates for the two patterns is limited by instability and transition to turbulence by observation of the flow streaklines.

Acknowledgements

This paper was a preliminary study for designing a test section for the mist/steam impingement cooling program supported by the U.S. Department of Energy under the contract number DE-FC21-92MC29061 and subcontract AGTSR 95-01-SR034. We appreciate the help from Dr. Tao Guo from General Electric Power System group.

References

Battaglia, F., Tavener, S.J., Kulkarni, A.K., Merkle, C.L., 1997. Bifurcation of low Reynolds number flows in symmetric channels. AIAA J. 35, 99–105.

Borgas, M.S., Pedley, T.J., 1990. Non-uniqueness and bifurcation in annular and planar channel flows. J. Fluid Mech. 214, 229–250.

Chiriac, V.A., Ortega, A., 2002. A numerical study of the unsteady flow and heat transfer in a transitional confined slot jet impinging on an isothermal surface. Int. J. Heat Mass Transfer 45, 1237–1248.

Chou, Y.J., Hung, Y.H., 1994. Impingement cooling of an isothermally heated surface with a confined slot jet. ASME J. Heat Transfer 116, 479–482.

Chung, Y.M., Luo, K.H., 2002. Unsteady heat transfer analysis of an impinging jet. ASME J. Heat Transfer 124, 1039–1048.

Garimella, S.V., Rice, R.A., 1995. Confined and submerged liquid jet impingement heat transfer. ASME J. Heat Transfer 117, 871–877.

Jambunathan, K., Lai, E., Moss, M.A., Button, B.L., 1992. A review of heat transfer data for single circular jet impingement. Int. J. Heat Fluid Flow 13, 106–115.

Jayanti, S., Hewitt, G.F., 1992. Numerical study of bifurcation in laminar flow in curved ducts. Int. J. Numer. Meth. Fluids 14, 253–1266.

Jiang, T.L., Shen, C., 1994. Numerical predictions of the bifurcation of confined swirling flows. Int. J. Numer. Meth. Fluids 19, 961–979.

Li, X., Gaddis, J.L., Wang, W., 2001. Mist/steam heat transfer in confined slot jet impingement. ASME J. Turbomach. 123, 161–167.

Martin, H., 1977. Heat and mass transfer between impinging gas jets and solid surfaces. Adv. Heat Transfer 13, 1–60.

Miyazaki, H., Silberman, E., 1972. Flow and heat transfer on a flat plate normal to a two-dimensional laminar jet issuing from a nozzle of finite height. Int. J. Heat Mass Transfer 15, 2097–2107.

Morris, G.K., Garimella, S.V., 1996. Orifice and impingement flow fields in confined jet impingement. ASME National Heat Transfer Conference, HTD-324, 101–106.

Orfi, J., Galanis, N., Nguyen, C.T., 1999. Bifurcation in steady laminar mixed convection flow in uniformly heated inclined tubes. Int. J. Numer. Meth. Heat Fluid Flow 9, 543–567.

Patankar, S.V., 1980. Numerical Heat Transfer and Fluid Flow. McGraw-Hill, New York.

Sezai, I., Aldabbagh, L.B.Y., 2004. Three-dimensional numerical investigation of flow and heat transfer characteristics of inline jet arrays. Numer. Heat Transfer; Part A: Applications 45, 271–288.

Sparrow, E.M., Wong, T.C., 1975. Impingement transfer coefficients due to initially laminar slot jets. Int. J. Heat Mass Transfer 18, 597–605.

van Heiningen, A.R.P., Mujumdar, A.S., Douglas, W.J.M., 1976. Numerical prediction of the flow field and impingement heat transfer caused by a laminar slot jet. ASME J. Heat Transfer 98, 654–658.